Excitation density dependence of photocurrent efficiency in low mobility semiconductors

Nir Tessler[a] and Noam Rappaport
Microelectronic and Nanoelectronic Center, Electrical Engineering Department, Technion Israel Institute of Technology, Haifa 32000, Israel

(Received 5 February 2004; accepted 31 March 2004)

We report numerical simulation of the charge transport in low mobility semiconductors under optical excitation. We choose the low mobility regime as it is typical of organic polymer semiconductor devices. We find that, contrary to common belief, the limiting factor for the photocurrent at high optical excitation density is the onset of space-charge limit and that bimolecular recombination is merely a result of the limited current. We also show that the power dependence of the photocurrent efficiency can be used to deduce which charge-carrier is the slow one and extract its mobility. © *2004 American Institute of Physics.* [DOI: 10.1063/1.1753082]

I. INTRODUCTION

Despite the fact that organic photocells[1–3] predates organic light emitting diodes[4,5] the latter have attracted much more attention and efforts leading to a more mature technology. The photocell field is currently showing a steady increase in reports concerning material synthesis[6,7] or material composite design[8–10] however, device oriented study and modeling are still rather scarce.[11–15] A recent, and relevant, study of photocells and the underlying mechanisms have been detailed in Refs. 13 and 15 however, the high excitation density regime did not receive much emphasis. In this article, we focus on high optical-excitation density regime and investigate the effect of the charge transport on the photocurrent extraction efficiency. We show that if the excitation density is raised to the point where the photocurrent external quantum efficiency starts to drop it is always due to space-charge effects imposed by the slow charge-carrier mobility. At the end of the article, we compare our numerical simulation with the experimental data presented in Ref. 13 and extract the slow charge carrier mobility in those devices.

II. NUMERICAL MODEL

To study the mechanisms underlying the operation of a photocell we have constructed a numerical model[16] that solves the following equations self-consistently:

$$\frac{\partial}{\partial t}n_e(z,t)=\frac{\partial}{\partial z}\left[D_e\frac{\partial}{\partial z}n_e(z,t)+\mu_e(E)n_e(z,t)E(z,t)\right]-R(z,t)+G(z,t), \tag{1}$$

$$\frac{\partial}{\partial t}n_h(z,t)=\frac{\partial}{\partial z}\left[D_h\frac{\partial}{\partial z}n_h(z,t)-\mu_h(E)n_h(z,t)E(z,t)\right]-R(z,t)+G(z,t), \tag{2}$$

$$\frac{d}{dz}E=\frac{q}{\epsilon}[n_h(z)-n_e(z)], \tag{3}$$

$$R=\frac{q}{\epsilon\epsilon_0}(\mu_e+\mu_h)n_e n_h, \tag{4}$$

$$J(z)=q\left[D_e\frac{\partial}{\partial z}n_e(z,t)+\mu_e(E)n_e(z,t)E(z,t)\right]-q\left[D_h\frac{\partial}{\partial z}n_h(z,t)-\mu_h(E)n_h(z,t)E(z,t)\right]. \tag{5}$$

Here, n_e and n_h are the electron and hole density, respectively. D_e and D_h are the electron and hole diffusion coefficients, which are given by $D_e=\mu_e kT/e$ and $D_h=\mu_h kT/e$ (where e is the unit of electrical charge). We do not take into account the effect of charge density on the mobility[17] or on the Einstein relation.[18] z is the distance from the cathode, R is the Langevin recombination rate, G is the optical generation rate, and J is the current flowing through the device. We assume that G is constant throughout the device which is valid as long as the electric field is not highly distorted in the device due to space-charge effects. The carrier population near the contacts is assumed to be at equilibrium with the contact and to avoid charge injection we have assumed a contact barrier of 0.6 eV for both electrodes. The excitation scheme used in this simulation is shown in Fig. 1. The device is composed of a single layer organic based material sandwiched between two electrodes. The electrode at the right facet of the device is assumed to be transparent and the light is shined onto the active layer through this electrode. The + and − symbols schematically describe electrons and holes and the arrows show the direction of the force applied by the electric field on these charges (hole to the right and electrons to the left).

III. SIMULATION RESULTS

A. Charge density and electric field distributions

The dashed line in Fig. 2 shows the excitation profile ($\exp[-z/L_{\text{abs}}]$, right axis) calculated assuming absorption length (L_{abs}) of 30 nm. The device length (distance between electrodes) is $d=100$ nm. The electron and hole density dis-

[a]Electronic mail: nir@ee.technion.ac.il

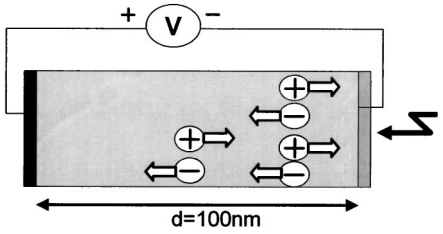

FIG. 1. Schematic description of the device configuration used in the simulation. It is a single layer photocell sandwiched between two electrodes. The electrode at the right facet of the device is assumed to be transparent and the light is shined onto the active layer through this electrode. The + and − symbols denote electrons and holes and the arrows show the direction of the force applied by the electric field on these charges.

tribution were calculated for a bias voltage such that the applied voltage (V_{appl}) together with the built in voltage (V_{bi}) result in a relative shift of the energy levels of 2 V ($V_{\mathrm{appl}}-V_{\mathrm{bi}}=-2$ V). We chose this bias to approximate the short circuit condition in a typical device. In these calculations $\mu_e=\mu_h=10^{-6}\,\mathrm{cm^2\,v^{-1}\,s^{-1}}$ and the absorbed power is varied between 0.03 mW cm^{-2} [Fig. 2(a)], 3 mW cm^{-2} [Fig. 2(b)], and 30 mW cm^{-2} [Fig. 2(c)]. To calculate the charge

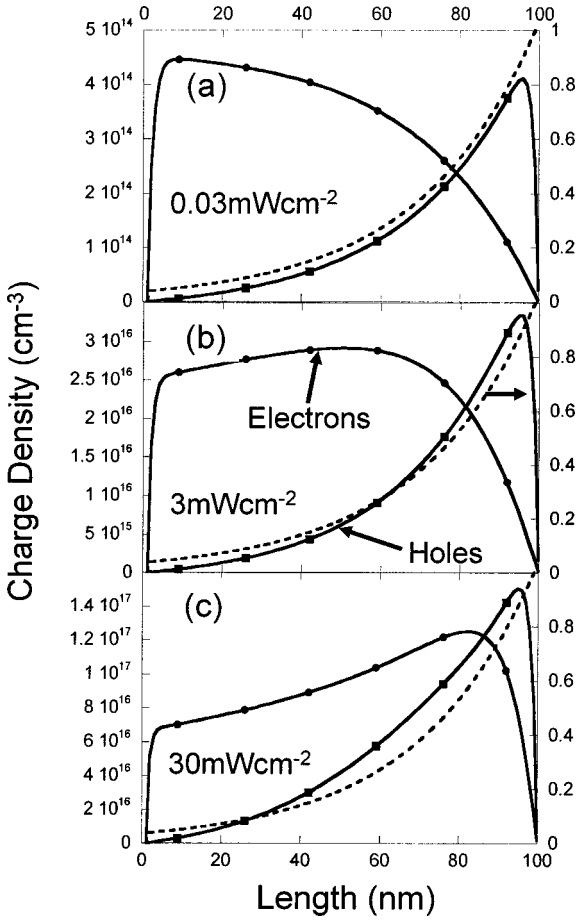

FIG. 2. Calculated electron (circle) and hole (square) density distribution as a result of a charge generation rate (dashed line, right axis). The applied bias is such that it tilts the bands by 2 V across the device ($V_{\mathrm{Appl}}-V_{\mathrm{bi}}=2$ V) having a length $d=100$ nm. (a) Excitation density $\sim$0.03 mW cm^{-2}, (b) excitation density $\sim$3 mW cm^{-2}, and (c) excitation density $\sim$30 mW cm^{-2}. Absorption length=30 nm.

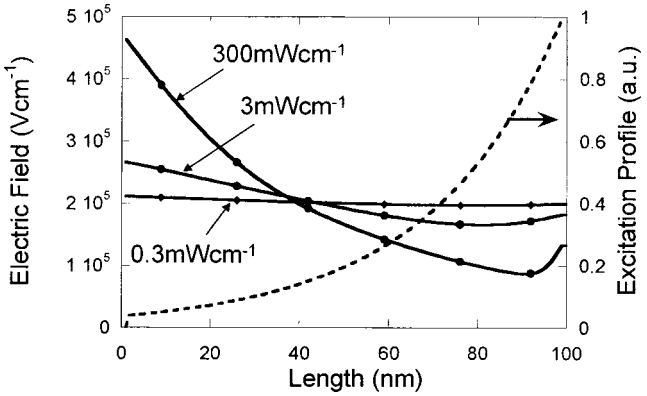

FIG. 3. Internal electric-field distribution as a function of the charge-generating optical excitation density. Note that at 0.3 mW cm^{-2} the excitation is too low to create significant space charge and hence the internal field remains constant throughout the device. Device parameters as in Fig. 2. Absorption length=30 nm.

generation rate we assume $\lambda=600$ nm and that every absorbed photon results in a dissociated electron-hole pair. Figure 2 shows that the bias pulls the electron (circles) and hole (squares) populations to their respective sides thus creating a space charge in the device. If the device is operated in the open-circuit mode this space charge would be giving rise to the output voltage (similar to the effect of charging of a capacitor). At the higher excitations [Figs. 2(b) and 2(c)] the density profile of the two charge carriers tend toward being similar indicating enhanced coulombic attraction between them. As we will show below, once the excitation density is high enough the space charge is sufficiently strong to alter the internal electric field and thus the device starts to operate in a space-charge-limited regime.

Figure 3 shows the electric field distribution within the device for several excitation densities. We note that, for the mobility values and bias voltage used, 3 mW cm^{-2} is a critical intensity beyond which space-charge effects become important to the point that the internal electric-field is changed. As Fig. 3 shows, to completely distort the electric field the generation rate (excitation power) must be very high. At this very high excitation regime our simulation is less exact due to the assumption that G is uniform across the device. However, as we will show below, most of the interesting information lies close to the critical point. We note that the space-charge phenomena and its effect on the charge-density distribution (or electric field) are different to that found in a light-emitting diode (LED) since the excitation scheme (boundary conditions) is different between the two cases. For example, the shape of the space-charge field (Fig. 3) is very different to that found in LEDs since the high charge density is not concentrated near the metallic contact (see Fig. 2) as it would be in the case of excitation through ohmic contacts used in LEDs (see Fig. 6 in Ref. 19). Nevertheless, we suggest the following: In a photocurrent cell one fixes the bias voltage and tries to drive as much current as possible through the device by optically injecting charges. However, just as in LEDs, the current achieved is that set by the space charge limit.

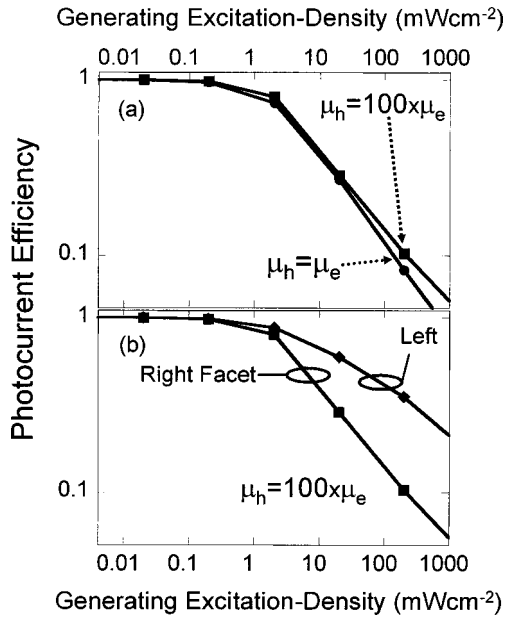

FIG. 4. Photocurrent extraction efficiency as a function of charge-generating excitation-power density for the same device as in Fig. 2. (a) The bottom line (circles) is for equal electron and hole mobility values and the upper line (squares) is for a hole mobility being enhanced by a factor of 10^2. (b) The bottom line (squares) is for excitation through the right facet (see Figs. 1 and 2) and the top curve (diamonds) is for excitation through the left facet. For both curves in (B) $\mu_h = 100\,\mu_e$. Absorption length=30 nm.

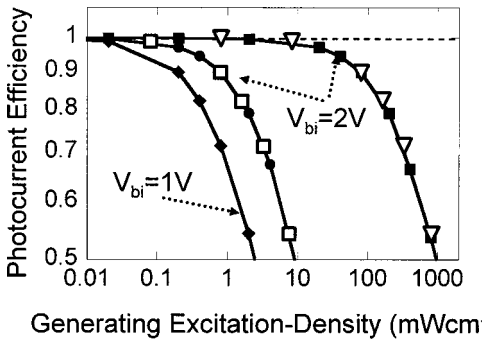

FIG. 5. Photocurrent extraction efficiency as a function of the charge-generating excitation-power density for the same device as in Fig. 2 but for absorption length $L_{\mathrm{Abs}} = 100$ nm. The left curve (diamonds) was calculated for $\mu_e = \mu_h = 10^{-6}\,\mathrm{cm^2\,v^{-1}\,s^{-1}}$ and $V_{\mathrm{bi}} = 1$ V ($V_{\mathrm{appl}} = 0$). The center curve (circles) was calculated for $\mu_e = \mu_h = 10^{-6}\,\mathrm{cm^2\,v^{-1}\,s^{-1}}$ and $V_{\mathrm{bi}} = 2$ V ($V_{\mathrm{appl}} = 0$). The right curve (squares) was calculated for $\mu_e = \mu_h = 10^{-4}\,\mathrm{cm^2\,v^{-1}\,s^{-1}}$ and $V_{\mathrm{bi}} = 2$ V ($V_{\mathrm{appl}} = 0$). The empty diamonds are the data points of the left curve but for an x-axis scaled up by 4 to mimic the V^2 effect. The empty triangles are the data points of the left curve but for an x-axis scaled up by 400 to mimic the μV^2 effect.

B. External quantum efficiency

To correlate the space charge with reduced photocurrent extraction efficiency we have repeated the calculation for a range of excitation powers and derived the resulting current. Figure 4(a) shows the normalized photocurrent efficiency (electrons out per photons in) as a function of optical excitation intensity. We plot the efficiency normalized to its low excitation limit to cancel out any possible dependence of the generation rate on the applied voltage. The lower curve, marked with circles, shows the case for $\mu_e = \mu_h = 10^{-6}\,\mathrm{cm^2\,v^{-1}\,s^{-1}}$ and the curve slightly above it, marked with squares, was calculated for $\mu_e = 10^{-6}\,\mathrm{cm^2\,v^{-1}\,s^{-1}}$ and $\mu_h = 10^{-4}\,\mathrm{cm^2\,v^{-1}\,s^{-1}}$. We note that the efficiency starts to drop at about 3 $\mathrm{mW\,cm^{-2}}$ which is the same intensity that corresponds to the onset of space-charge effects in Fig. 3. Namely, the factor that limits the exit rate of charges (current) from the device is indeed the onset of space charge. Once this is set the charges must ''find'' another channel to ''exit'' through and thus the electron-hole recombination rate starts to rise (as a result of the space-charge limit). The curve marked with squares is very similar to the one marked with circles showing, as expected, that the space-charge-limited current is set by the lower mobility carrier. It is interesting to note that although by changing the hole mobility from 10^{-6} to $10^{-4}\,\mathrm{cm^2\,v^{-1}\,s^{-1}}$ the recombination rate was enhanced by two orders of magnitude [see Eq. (4)] the efficiency curve was hardly altered indicating that the charge-recombination is not the limiting factor and is merely a result of space-charge limit on the output current. Figure 4(b) compares two excitation profiles for mobility values of $\mu_e = 10^{-6}\,\mathrm{cm^2\,v^{-1}\,s^{-1}}$ and $\mu_h = 10^{-4}\,\mathrm{cm^2\,v^{-1}\,s^{-1}}$. The curve marked with squares is identical to the one shown in Fig. 4(a) using the excitation scheme as in Fig. 1. The top curve, marked with diamonds, was calculated for an excitation profile resulting from shining the light onto the device through the slow-carrier (electron) collecting electrode (left facet in Fig. 1). We note that such an extreme change in the excitation profile changes the shape of the photocurrent efficiency but it barely changes the point where space-charge effects start to play a role. Any other excitation profile resulting from a longer absorption length will be between these two extreme values (not shown here).

C. Space-charge limit

Based on the above we propose that at low excitation density the current is photo-injection limited and the efficiency is determined by the free-charge generation-efficiency. At higher excitation density the separation of the electron and hole population by the built-in (and/or applied) voltage creates a space charge that is large enough to alter the electric field. Once this occurs the photocurrent becomes space-charge limited and the residence time of the carriers in the device is increased thus enhancing the recombination rate. If this physical picture is correct then we should be able to use the analytic form for space-charge-limited current in LEDs ($J_{\mathrm{SCL}} = 9/8\epsilon\mu V^2/d^3$) to find clues as to what may affect the short circuit current or maybe even extract the mobility value of the slow charge carrier. We do not suggest that the photocurrent would follow the Mott–Gurney law for space charge but rather that the upper limit (at high excitation powers) is proportional to the space-charge current. If this is so, the saturation current or the efficiency curves would scale similarly to the space charge limited current. For example, it would be interesting to find out if the excitation density at which space-charge effects start to take place scales as μV^2 ($V \equiv V_{\mathrm{appl}} - V_{\mathrm{bi}}$). To this extent, we plot in Fig. 5 the photocurrent efficiency assuming an absorption length of 100 nm and $V_{\mathrm{appl}} - V_{\mathrm{bi}} = -1$ V $\mu_e = \mu_h$

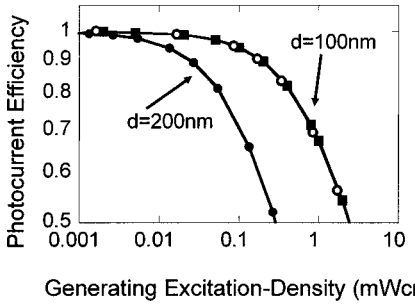

FIG. 6. Photocurrent extraction efficiency as a function of the charge-generating excitation-power density. $V_{bi}=1$ V ($V_{appl}=0$) and the absorption length=100 nm. The left curve (circles) was calculated for a device of a length $d=200$ nm and the right curve (squares) was calculated for the same device as in previous figures ($d=100$ nm). The empty circles are the data points for the $d=200$ nm device but with an x-axis scaled up by a factor of $2^3=8$.

$=10^{-6}\,\mathrm{cm^2\,v^{-1}\,s^{-1}}$ (filled diamonds), $V_{appl}-V_{bi}=-2$ V $\mu_e=\mu_h=10^{-6}\,\mathrm{cm^2\,v^{-1}\,s^{-1}}$ (filled circles), and $V_{appl}-V_{bi}=-2$ V $\mu_e=\mu_h=10^{-4}\,\mathrm{cm^2\,v^{-1}\,s^{-1}}$ (filled squares). The calculation is shown only down to half of the maximum efficiency value as this is the region that may be experimentally accessible. If the idea of space-charge limit is valid then we should be able to shift the left curve to match any of the other curves by scaling the x-axis according to μV^2. The empty diamonds are the data points from the calculation for $V_{appl}-V_{bi}=-1$ V $\mu_e=\mu_h=10^{-6}\,\mathrm{cm^2\,v^{-1}\,s^{-1}}$ but plotted against an x-axis multiplied by $(2/1)^2=4$. Namely, these points should represent an enhancement of the built in voltage by a factor of 2. The empty triangles are again the same data points as in the left curve but now plotted against an x-axis multiplied by 400. Namely, these points should now represent an enhancement of the built in voltage by a factor of 2 and of the mobility value by a factor of a 100. The overlap achieved using the scaling low of μV^2 is perfect.

Having found this agreement with the μV^2 we carry on to check the $1/d^3$ scaling (see Fig. 6). Figure 6 shows the results of a calculation for $V_{appl}-V_{bi}=-1$ V, $\mu_e=\mu_h=10^{-6}\,\mathrm{cm^2\,v^{-1}\,s^{-1}}$, absorption length of 100 and two device thickness, 100 and 200 nm. As the figure shows, the two curves do scale and the length scaling factor is $dF=8$ which is the length ratio to the third. We note that in our simulations we have not introduced any assumption regarding space-charge effects and the importance of space charge is a result of the self-consistent model we use. The importance of space-charge effects has also been addressed in Ref. 15 for double layer device where the effect is slightly different. The excellent fit with the μV^2 scaling and the $1/d^3$ scaling suggest that one should be able to develop an analytic expression for the curves shown in Figs. 5 and 6 however, we have not been able to do so.

IV. METHOD FOR EXTRACTING THE SLOW-CARRIER MOBILITY VALUE

Finally, we demonstrate a method for extracting the slow charge-carrier mobility. We implement the method on the data reported by Huynh *et al.* in Ref. 13, Fig. 7. In Table I we show the values that were used to plot photocurrent efficiency that was shown in Fig. 5 for the case of $V_{appl}-V_{bi}=-1$ V $\mu_e=\mu_h=10^{-6}\,\mathrm{cm^2\,v^{-1}\,s^{-1}}$. The two left columns in Table II show the data we have manually extracted from Fig. 7 in Ref. 13. To place this data on the same footing of the simulation we have deduced the (average) maximum value of the photocurrent efficiency (0.52). We multiply this value by the power density reported in Ref. 13 to deduce power density that gave rise to dissociated electron-hole pair or the ''generating power'' (first column on the right side of Table II). Next, we normalize the photocurrent efficiency by this maximum average value to arrive at the right most column. Figure 7 shows the simulated data from Table I (filled squares) as well as the normalized data extracted from Fig. 7 in Ref. 13 and shown in Table II (filled circles). It is obvious that to bring the simulation data toward the measured data one has to scale up the x-axis of the simulation data. The empty squares show the same data as in Table I but the left column (x-axis) was multiplied by a factor (MF) of MF=40. We note that the functional form is practically identical. To extract the mobility value we also need to know the built-in voltage, the device length, and the excitation wavelength in the two cases.

TABLE I. The data points calculated for $d=100$ nm, $\mu=10^{-6}\,\mathrm{cm^2\,V^{-1}\,s^{-1}}$ and $V_{bi}=-1$ V.

(Absorbed power [mW cm^{-2}])×(maximum efficiency)	Normalized efficiency
0.002 001 4	1.0000
0.005 003 4	0.996 99
0.020 014	0.989 21
0.050 034	0.971 17
0.100 07	0.944 77
0.200 14	0.898 27
0.400 27	0.822 29
0.800 54	0.714 87
0.999 88	0.674 59
2.0014	0.542 95
4.0027	0.416 26

TABLE II. The data as extracted from Ref. 13 (left columns) and after applying the procedure outlined in the text (right columns).

Manually extracted data from Ref. 13		Modified data	
Power [mW cm^{-2}]	External quantum efficiency	Power×Average maximum efficiency	Normalized efficiency
0.150 00	0.515 00	0.078 000	0.990 38
0.300 00	0.515 00	0.156 00	0.990 38
0.450 00	0.500 00	0.234 00	0.961 54
0.770 00	0.510 00	0.400 40	0.980 77
1.5000	0.510 00	0.780 00	0.980 77
3.0000	0.535 00	1.5600	1.0288
4.5000	0.530 00	2.3400	1.0192
7.0000	0.510 00	3.6400	0.980 77
11.000	0.480 00	5.7200	0.923 08
18.000	0.460 00	9.3600	0.884 62
37.000	0.400 00	19.240	0.769 23
60.000	0.375 00	31.200	0.721 15
100.00	0.320 00	52.000	0.615 38
160.00	0.290 00	83.200	0.557 69

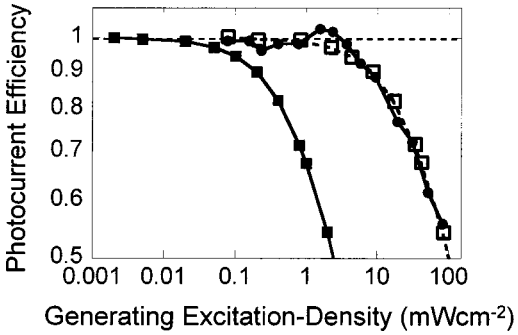

FIG. 7. Photocurrent extraction efficiency as a function of charge-generating excitation-power density. The curve marked with full squares is based on Table I. The points marked with full circles are the data points taken from Fig. 7 in Ref. 13 and normalized (Table II). The empty squares are the data points taken from Table I but with the *x*-axis scaled up by a factor of 40.

According to Ref. 13, the device used had a built-in voltage of $V_{bi}=0.7\,V$, excitation was at ~500 nm, and its length[20] $d=220\,nm\pm10\,nm$. Therefore the slow carrier mobility can be expressed as $\mu_{exp}=10^{-6}MF/V_{bi}^2dF\times\lambda F=10^{-6}40/0.7^2(220/100)^3500/600\cong5\times10^{-4}$ $cm^2\,v^{-1}\,s^{-1}$. In order to deduce if the slow carriers are electrons or holes one would need to repeat the experiment in Ref. 13 for a different absorption length and check if the curve slightly shifts to higher excitation or lower excitation density values [see Fig. 4(b)]. Using the mobility parameter extracted above we can now use the numerical model to calculate the current density as a function of light intensity for the device used in Ref. 13. Figure 8 shows the result of such calculation and the excellent agreement with the measurement shown in Fig. 8 of Ref. 13 strengthens the validity of our mobility extraction procedure.

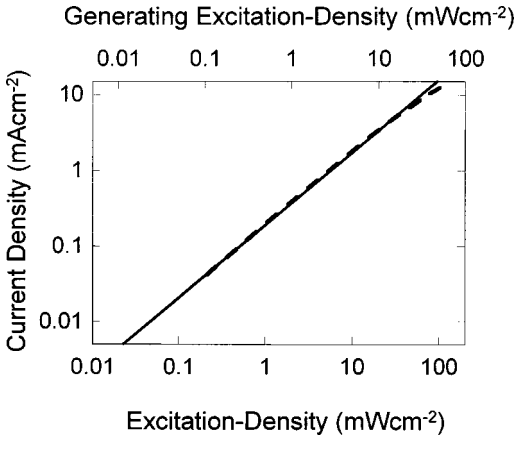

FIG. 8. Current density as a function of ~500 nm light intensity. The calculation was carried out for the device in Fig. 7 of Ref. 13 using the mobility value extracted here ($5\times10^{-4}\,cm^2\,v-1\,s^{-1}$). The dashed line is the calculation and the full line if a power-law fit with a slope of 0.96. The agreement with Fig. 8 of Ref. 13 is excellent.

V. CONCLUSIONS

To conclude, we have shown that the factor limiting the efficiency of photocells operating in current-mode at high optical excitation density is the onset of space-charge effects. This implies that to arrive at better device performance one must enhance the mobility of both electrons and holes and not only of holes (which is typically easier). We have also shown that failing to achieve high electron mobility one can partially compensate for that by shining the light into the device through the electron collecting electrode [Fig. 4(b)], emphasizing the need for a transparent electron injecting/collecting electrode. Finally, we propose that the onset of space-charge effects is a good measure for the slow charge carrier mobility and the shape of the curve can tell us if we are measuring electrons or holes mobility. This procedure was implemented on data measured by others.[13]

Note added in proof: We have recently developed analytical expressions describing separately the effects of space charge and of charge recombination and found that, for Langevin type recombination, both mechanisms exhibit V^2/d^3 dependence and have a very similar onset power.

ACKNOWLEDGMENT

We acknowledge support by the EU through Contract no. G5RD-CT-2001-00577 OPAMD

[1] C. W. Tang, Appl. Phys. Lett. **48**, 183 (1986).
[2] C. J. Brabec and S. N. Sariciftci, Monatsch. Chem. **132**, 421 (2001).
[3] W. U. Huynh, J. J. Dittmer, and A. P. Alivisatos, Science **295**, 2425 (2002).
[4] C. W. Tang and S. A. VanSlyke, Appl. Phys. Lett. **51**, 913 (1987).
[5] J. H. Burroughes, D. D. C. Bradley, A. R. Brown, R. N. Marks, K. Mackay, R. H. Friend, P. L. Burns, and A. B. Holmes, Nature (London) **347**, 539 (1990).
[6] G. Yu, J. Wang, J. McElvain, and A. J. Heeger, Adv. Mater. (Weinheim, Ger.) **10**, 1431 (1998).
[7] M. Gritzel and K. Kalyanasundaram, Curr. Sci. **66**, 706 (1994).
[8] A. C. Arias, J. D. Mackenzie, R. Stevenson, J. J. M. Halls, M. Inbasekaran, E. P. Woo, D. Richards, and R. H. Friend, Macromolecules **34**, 6005 (2001).
[9] J. J. M. Halls, C. A. Walsh, N. C. Greenham, E. A. Marseglia, R. H. Friend, S. C. Moratti, and A. B. Holmes, Nature (London) **376**, 498 (1995).
[10] G. Yu, J. Gao, J. C. Hummelen, F. Wudl, and A. J. Heeger, Science **270**, 1789 (1995).
[11] M. G. Harrison, J. Gruner, and G. C. W. Spencer, Phys. Rev. B **55**, 7831 (1997).
[12] L. A. A. Pettersson, L. S. Roman, and O. Inganas, J. Appl. Phys. **86**, 487 (1999).
[13] W. U. Huynh, J. J. Dittmer, N. Teclemariam, D. J. Milliron, A. P. Alivisatos, and K. W. J. Barnham, Phys. Rev. B **67**, 115326 (2003).
[14] H. Hoppe, N. Arnold, N. S. Sariciftci, and D. Meissner, Sol. Energy Mater. Sol. Cells **80**, 105 (2003).
[15] C. M. Ramsdale, J. A. Barker, A. C. Arias, J. D. Mackenzie, R. H. Friend, and N. C. Greenham, J. Appl. Phys. **92**, 4266 (2002).
[16] D. J. Pinner, R. H. Friend, and N. Tessler, J. Appl. Phys. **86**, 5116 (1999).
[17] Y. Roichman and N. Tessler, Synth. Met. **135–136**, 443 (2003).
[18] Y. Roichman and N. Tessler, Appl. Phys. Lett. **80**, 1948 (2002).
[19] Y. Preezant, Y. Roichman, and N. Tessler, J. Phys.: Condens. Matter **14**, 9913 (2002).
[20] W. U. Huynh (private communication).